Model Predictive Path Integral Approach for Trajectory Guidance of Rotorcraft Shipboard Landing

J. V. R. Prasad
Professor

Vinodhini Comandur
Ph.D. Student

Robert Walters
Graduate Student

David Guerrero
Flight Test Engineer (USAF)

School of Aerospace Engineering,
Georgia Institute of Technology
Atlanta, GA, USA

ABSTRACT

Rotorcraft shipboard landing continues to be challenging due to increased pilot workload in dealing with effects of ship air wake turbulence on vehicle motion and random ship motion. Some of the recent work has proposed a pilot assist function for reduced pilot workload using model predictive control methods. This paper explores the use of a recently developed Model Predictive Path Integral (MPPI) method based on a stochastic optimal control framework for trajectory guidance solution to the shipboard landing problem. First, a proof-of-concept study is presented by applying the MPPI method to a simple point mass approximation of helicopter dynamics represented in the form of a first-order command acceleration model, representative of helicopter trajectory motion in the vertical plane. Next, the MPPI method is used in conjunction with a six degrees-of-freedom linear model of a helicopter in order to gain further insight into the applicability of the MPPI framework to the rotorcraft shipboard landing problem. The paper concludes with key observations and inferences gained in this study.

NOTATION

A State matrix
a Acceleration in inertial frame (ft/s^2)
B Control or Input matrix
C Output matrix
F Weighting function
J Performance measure or index
M Number of random control vectors or trajectories
p Body roll rate (rad/s^2)
Q Error weighting matrix
q Body pitch rate (rad/s^2)
R Control weighting matrix
r Body yaw rate (rad/s^2)
t Time (s)
u Control input vector (percent)
u_b Helicopter body velocity along body x-axis (ft/s)
u_m Initial guess for control input
v Gaussian noise sample
v_b Helicopter body velocity along body y-axis (ft/s)
w_b Helicopter body velocity along body z-axis (ft/s)
X Inertial position in inertial x-axis (ft)
Y Inertial position in inertial y-axis (ft)
Z Inertial position in inertial z-axis (ft)
Δ Discrete step (time)
δ_a Lateral cyclic input (percent)
δ_b Longitudinal cyclic input (percent)
δ_c Collective input (percent)
δ_p Pedal input (percent)
ϕ Roll attitude (rad)
θ Pitch attitude (rad)
ψ Yaw attitude (rad)
σ Standard deviation
τ Time constant (s)

Subscripts
f Final (time)
h Physical quantity associated with the helicopter/vehicle
i Trajectory or random control element number
j Current time instant
ref Reference
s Physical quantity associated with the ship
win Window
0 Initial (time)

INTRODUCTION

Shipboard launch and recovery operations continue to be one of the more challenging flight regimes for rotorcraft. Pilot workload issues can often be the limiting factor when defining allowable sea state and wind-over-deck (WOD) conditions for a helicopter and ship combination. The challenges associated with the recovery phase are how to deal with random deck motions, unsteady aerodynamic conditions due to interactions between airflow over the ship and wake due to the rotor of the

Presented at the AHS International 74th Annual Forum & Technology Display, Phoenix, Arizona, USA, May 14-17, 2018.

vehicle, and degraded visual environments for achieving a smooth touch down.

Several studies have been conducted to tackle the shipboard landing task by developing controllers for autonomous landing, ship deck motion prediction algorithms and incorporating ship air wake turbulence models. References 1 through 4 have performed non-real-time simulations of shipboard operations with workload estimation from pilot models. Vision-based control has been tested in Refs. 5 and 6. Flight controllers for ship approach and landing have been presented in Refs. 7 and 8, while Ref. 9 presents objective functions for optimal path guidance for shipboard landing. Most past investigations have explored, with limited success, either ship deck motion feedback to form a closed loop system or provide a pilot assist function for reduced pilot workload using model predictive control (MPC) methods and statistical predictions of deck position and velocity states at a future time.

Because of the stochastic nature of ship deck motions and air wake effects, it is imperative that these effects are included for synthesizing satisfactory solutions to the shipboard landing problem. Solutions to stochastic problems are computationally unwieldy for real time applications. Although MPC methods are promising, their dependence on explicit optimization is a major drawback. Hence, they are not parallelizable, making them very difficult for real-time implementation without a significant sacrifice in solution fidelity. One of the key challenges in developing real-time guidance solutions to the shipboard recovery problem is the choice of the computational scheme.

Indirect methods, such as Model Predictive Path Integral (MPPI) approach (Ref. 10), obtain solutions through implicit optimization by averaging across a stochastic sample of trajectories, and hence, are parallelizable for real time implementation. The focus of the paper is a proof-of-concept study using the MPPI approach to develop real time guidance solutions for a rotorcraft shipboard landing task, while accounting for random deck motions.

MPPI APPROACH FOR OPTIMIZATION

Method Overview

The MPPI approach evaluates the appropriate control based on a performance measure using an onboard model of the vehicle dynamics. Using an initial estimate u_m for the control vector over initial time t_o to the final time t_f, several sample control vectors (u_i's) are constructed as random perturbations (du_i) from u_m.

$$u_i = u_m + du_i, \quad i = 1 \; to \; M \tag{1}$$

where M is the number of sample control vectors. The random control perturbations are limited to be within certain values. For each u_i, the corresponding sample trajectory (x_i) is obtained using the onboard model, and simultaneously, the chosen performance index (J_i) for the sample trajectory is evaluated. Next, the updated control vector u_p is obtained using the weighted averaging of du_i as

$$u_p = u_m + \frac{1}{M}\sum_{i=1}^{M}(du_i)e^{-J_i} \tag{2}$$

The inclusion of exponential weighting allows the control update u_p to be heavily biased towards trajectories with lower cost values J_i, and thus implicitly forcing u_p towards the optimal solution. This process is repeated by replacing u_m in Eq. 1 with the control update u_p from Eq. 2. At each time instant, the three main steps – 1) the generation of random control vectors and the corresponding trajectories, 2) evaluation of performance measure for each trajectory, and 3) stochastic averaging to obtain updated control, are repeated again if the number of rejected trajectories exceed 90% of M, and the control perturbation magnitude is increased for the next cycle. Trajectories which yield large terminal errors are rejected, which has been elaborated further in the subsequent sections. Thus, the averaging performed in Eq. 2 facilitates rapid convergence (Ref. 10), typically in a couple of iterations, to the optimal solution.

Initial Study (Ship deck without Random Motion)

The initial study considers a simplified representation of the vehicle using a point mass approximation with two independent degrees of freedom and commanded accelerations along the inertial X- and Z-axis as control variables. This simplified representation allows the assessment of the MPPI solution fidelity by comparing it with the theoretical solution for the ideal case, i.e., no random ship deck motion and no air wake effects. Additionally, the closed form optimal control solution for the ideal case is used as the starting estimate for the case when random deck motion and air wake effects are included in the MPPI solution.

The dynamic model of the vehicle motion along the vertical axis is assumed to be of the form

$$\begin{bmatrix}\dot{z}\\ \dot{w}\\ \dot{a}\end{bmatrix} = \begin{bmatrix}0 & 1 & 0\\ 0 & 0 & 1\\ 0 & 0 & -\frac{1}{\tau}\end{bmatrix}\begin{bmatrix}z\\ w\\ a\end{bmatrix} + \begin{bmatrix}0\\ 0\\ \frac{a_c}{\tau}\end{bmatrix} \tag{3}$$

A similar model is used for representing motion along the horizontal axis, where τ (set to 1*s* in this study) is the time constant of an assumed trajectory controller with command acceleration as input. Both X and Z axes models are evaluated separately as they are independent from one another for this simple case. It is also important to note that the same model is used for the onboard model (prediction model) as well as the truth model. Here, the commanded acceleration a_c represents the control u. The initial estimate u_m is calculated as an optimal solution by minimizing the control effort (a quadratic performance index) with the terminal constraint of matching the average position z_s and the velocity w_s of the ship at a selected final time in the following manner:

$$u_m(t) = min_{a_c}(J) \quad (4)$$

$$J = \int_{t_0}^{t_f} \frac{1}{2} a_c{}^2(t)dt \quad (5)$$

$$z_h(t_f) = z_{s_{average}}(t_f), w_h(t_f) = w_{s_{average}}(t_f) \quad (6)$$

The solution to the optimization problem defined by Eqs. 4 through 6 with the assumed linear model of Eq. 3 can be obtained using optimal control theory. The theoretical optimal solution forms a good basis for evaluating the workings of the MPPI method. The fidelity of the MPPI solution is checked by fixing the terminal conditions (assuming the ship is moving at a constant velocity only and the random motions of ship deck are not included, which is also considered for the optimal control theory based solution), in which case the MPPI solution should be close to the optimal control theory based solution.

The landing phase considered in this part of the study is as follows: At the start time (t_0), the vehicle is in level flight with a speed of 55 knots (95.4 ft/s) and its location at 100 ft above and 1100 ft behind the ship deck. The ship is moving at a constant speed of 19.8 knots (33.5 ft/s). The total landing time (t_f-t_0) is 40 *s*. A sketch of the assumed landing phase in medium sea state is shown in Fig. 1.

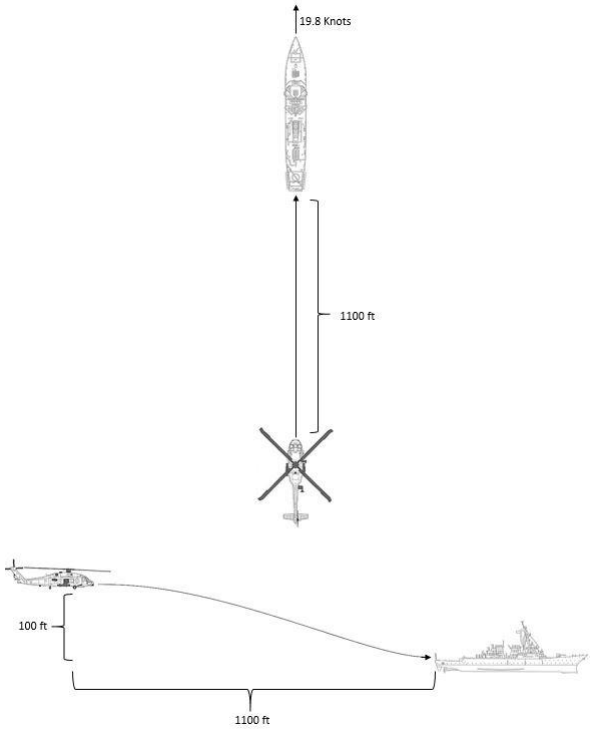

Figure 1. Symmetric landing phase (zero lateral offset).

In the MPPI solution, a set of M random control vectors (*M=100*) is generated from the start of the vehicle approach to the selected landing time t_f *=40 s* (t_0 *=0 s*) as per Eq. 1. The random control perturbations are limited to be within the applicable acceleration command (control) limits (set to 10% for both X and Z axes here). Then, vehicle trajectories are calculated by applying the selected set of random control vectors of Eq. 1 in Eq. 3. If any trajectory results in a terminal position error (difference between the ship deck position and vehicle position) more than 5 ft and terminal velocity error more than 3 ft/s, it is rejected. Simultaneously, for each of the acceptable trajectories, the value of the selected performance index (J_i) is evaluated as

$$J_i = \int_{t_j}^{t_f} \frac{1}{2} u_i{}^2(t)dt + F\left(\left(z_h(t_f) - z_{s_{avg}}(t_f)\right)^2 + \left(w_h(t_f) - w_{s_{avg}}(t_f)\right)^2\right) \quad (7)$$

F, mentioned in Eq. 7, is a time dependent weighting function, logarithmically spaced from $10^{-0.5}$ to $10^{2.5}$, to trade between path cost and terminal cost in the solution. This function exponentially favors terminal constraints rather than path cost as the vehicle approaches the ship deck. An exponentially weighted averaging (Eq. 2) is used to obtain a new estimate of the control a_c. z_h and w_h represent the predicted position and velocity of the vehicle respectively, in the vertical axis, while z_{s_avg} and w_{s_avg} represent the average position and velocity of the ship (without random deck motion). A similar performance index is evaluated for the horizontal axis using X axis position and velocity for terminal cost.

As explained earlier, if the number of rejected trajectories are more than 90 at any time instant, the process iterates between Eqs. 1, 7 and 2 for a converged update of $a_c(t)$ (u_p), i.e. optimal acceleration command for the fixed ship position and velocity at the terminal time by increasing the control perturbation magnitude by 10% for each iteration. A limit is placed on the maximum number of iterations at 9 to save on computational time. It is observed that the Z axis performs just a single iteration at each time step while for X axis, the number of iterations required initially is 9 and then converges to 1 towards the end of the landing time. The converged command acceleration u_p resulting from Eq. 2 is then used to integrate the vehicle dynamics (truth model) from current time t_0 to $t_0 + \Delta t$, where Δt is a preselected time increment (say $\Delta t = 0.1$ *s*). The new position and velocity of the vehicle at $t_0 + \Delta t$ is used as the starting vehicle state for the onboard model. A new optimal control solution valid from $t_0 + \Delta t$ to t_f from Eqs. 1 and 2 is generated. The above process is repeated to obtain an optimized solution over the time horizon from $t_0 + 2\Delta t$ to t_f, and next from $t_0 + 3\Delta t$ to t_f, and so on. In this manner, the time horizon for optimization continues to shrink until t_f (shrinking horizon method). Each time, the optimized control u_p is applied only over a time interval of Δt. In the actual application, the optimized solution is provided as a guidance trajectory to the pilot to follow, which is continuously updated at a selected rate using each time a new random set of ship deck position and velocity at the terminal time.

The optimal control theory based solution and the MPPI solution are compared in Figs. 2 through 4. It is seen from these results that the MPPI solution is very close to the

optimal control theory based solution for this ideal case. Any differences seen in Figs. 2 through 4 are due to errors arising from numerical integration and the differences in the way terminal constraints are treated by the two approaches. While the optimal control theory based solution can enforce exact matching of the terminal constraints, the MPPI solution treats the terminal constraints through a terminal cost term in the performance index.

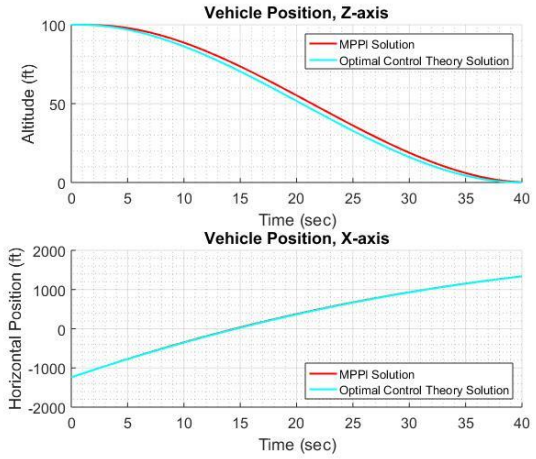

Figure 2. Vehicle positions (MPPI and optimal control solutions) in the X, Z-axes [point mass model].

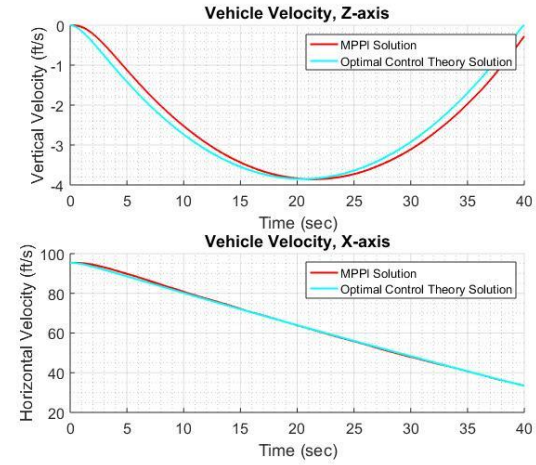

Figure 3. Vehicle velocities (MPPI and optimal control solutions) in the X, Z-axes [point mass model].

Initial Study (Ship deck with Random Motion)

This case considers a moving ship deck with random motion as a function of sea state, which is accounted for in the terminal constraint. The ship motion is generated using a ship motion model described later in this section. The methodology for this case is the same as that described in the fixed ship deck case with the performance index now accounting for random ship deck motion in the terminal cost as shown in Eq. 8.

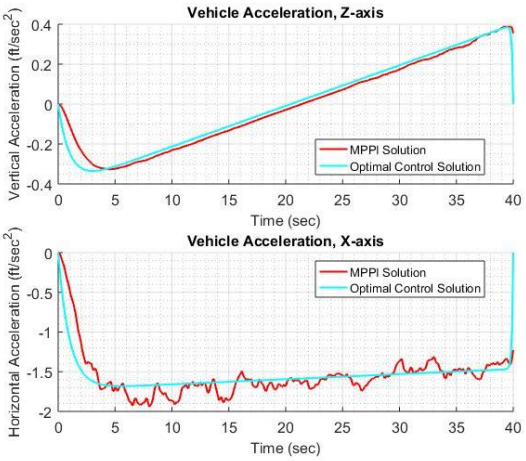

Figure 4. Vehicle accelerations (MPPI and optimal control solutions) in the X, Z-axes [point mass model].

$$J_i = \int_{t_j}^{t_f} \frac{1}{2} {u_i}^2(t)dt + F\left(\left(z_h(t_f) - z_s(t_f)\right)^2 + \left(w_h(t_f) - w_s(t_f)\right)^2\right) \quad (8)$$

Table 1. DDG-51 Combatant ship representative motion statistics, heave as dominant motion.

		Sea State		
		Low	**Medium**	**High**
Horizontal Velocity (ft/sec)	RMS	0.18	0.36	0.73
	Mean	8.1	33.5	50.0
	Max/Min	8.8/7.5	34.5/32.0	51.7/46.1
Lateral Velocity (ft/sec)	RMS	0.74	0.89	1.76
	Mean	0.0	0.0	0.0
	Max/Min	2.5/-2.1	3.2/-3.4	6.3/-5.6
Vertical Acceleration (ft/sec^2)	RMS	1.14	2.43	5.13
	Mean	0.0	0.0	0.0
	Max/Min	3.5/-4.2	8.3/-8.6	16.8/-19.2

In Eq. 8, z_s and w_s represent the position and velocity of the ship with random deck motion. Note that the generated random ship deck position and velocity are used for all M trajectories in this part of the MPPI solution. The random control perturbations are kept at 10% for both axes. As incorporated earlier, at every time step, any trajectory which results in the terminal position error more than 5 ft and terminal velocity error more than 3 ft/s is eliminated.

Ship deck Motion Model

The ship motion model used in this study is representative of a destroyer type ship such as the DDG-51. The US Navy Office of Naval Research (ONR), Naval Surface Warfare Center Carderock Division (NSWCCD) provided the statistical data required to generate the ship motion in the x- and z-axes. Ship motion in the z-axis (heave motion) is generated from random acceleration with mean and standard deviation of the selected sea state for the DDG-51 ship. The ship's forward velocity is selected from 4.8 knots (8.1 ft/s), 19.8 knots (33.5 ft/s), or 29.6 knots (49.98 ft/s) depending on low, medium or high sea state, respectively. Surge and sway motions are randomly generated with the standard deviation for the selected sea state. The representation is shown in Table 1.

Results and Analysis

Figures 5 through 9 depict the results for a moving ship with random ship deck motion for medium sea state. As shown in Fig.1, the vehicle starts the landing phase from a height of 100 ft above and 1100 ft behind the ship deck with an X velocity of 95.4 ft/s. The discrete time step is 0.1 s for both axes.

The vehicle positions as obtained from MPPI reach the ship deck within 1 ft at the terminal time. The optimal control

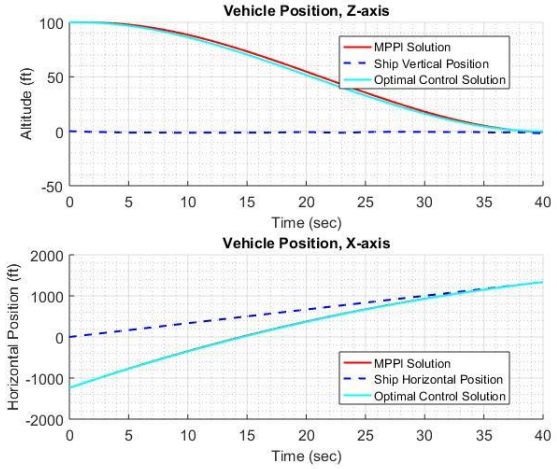

Figure 5. Vehicle positions (MPPI and optimal control solutions) and ship deck positions in the X, Z-axes for random ship deck motion [point mass model].

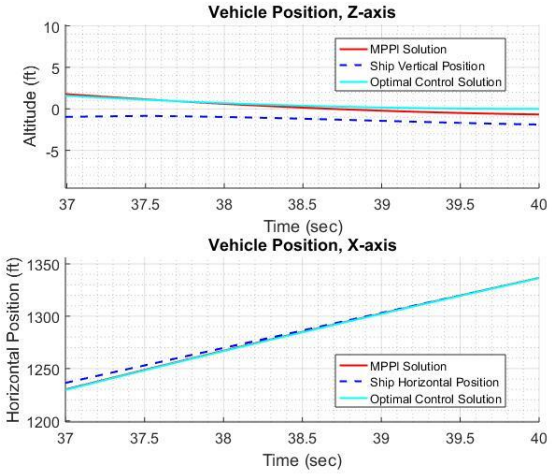

Figure 6. Vehicle positions (MPPI and optimal control solutions) and ship deck positions in the X, Z-axes for random ship deck motion in the last three seconds [point mass model].

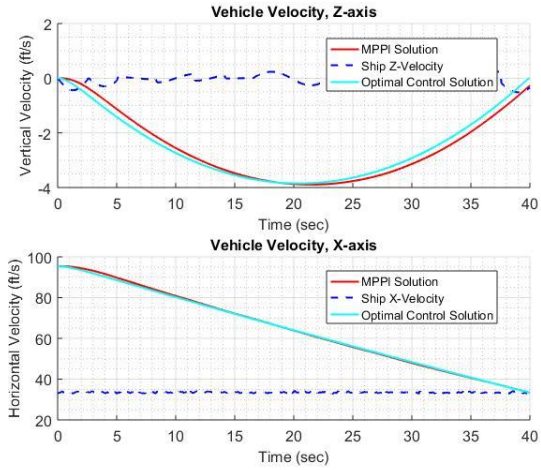

Figure 7. Vehicle velocities (MPPI and optimal control solutions) and ship deck velocities in the X, Z-axes for random ship deck motion [point mass model].

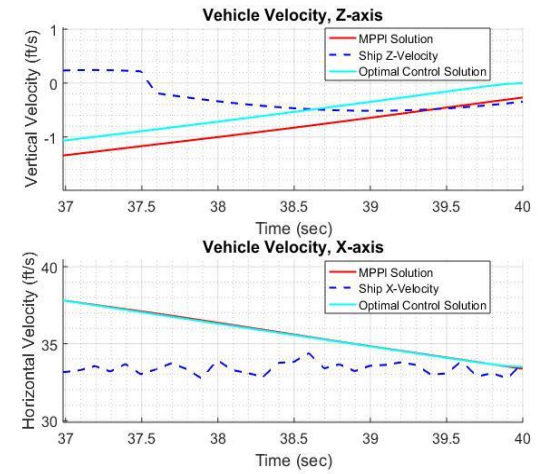

Figure 8. Vehicle velocities (MPPI and optimal control solutions) and ship deck velocities in the X, Z-axes for random ship deck motion in the last three seconds [point mass model].

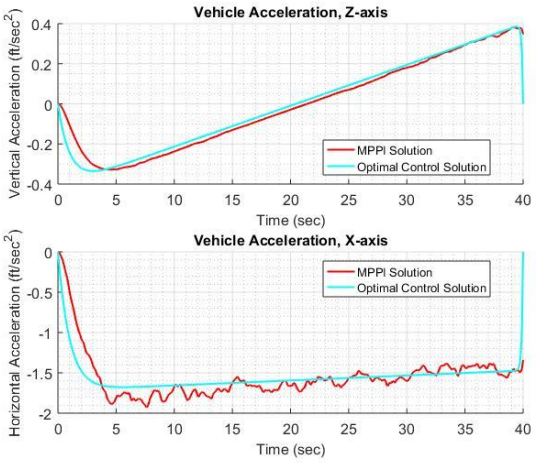

Figure 9. Vehicle accelerations (MPPI and optimal control solutions) in the X, Z-axes for random ship deck motion [point mass model].

solution shown is obtained for a ship deck without random motion.

Figure 7 shows the velocity profiles generated from MPPI for the case with random ship deck motion and they are compared with the optimal control solution without random motion of the ship deck. The velocity errors between the vehicle and the ship deck at the terminal time are within 1 ft/s.

Figure 9 depicts the vehicle accelerations as obtained from MPPI for ship with random deck motion and optimal control theory solution without random deck motion.

The summary results for all the sea states, averaged over 30 simulations for each sea state, are presented in Table 2. It is observed that the errors are within acceptable limits for all the sea states. The average number of usable trajectories indicates how many trajectories out of 100 are acceptable, i.e. fall within the error limits of 5 ft in position and 3 ft/s in velocity. Although the number of usable trajectories is similar in Z axis for all sea states, the number of usable trajectories in X axis increases with sea state. This is because as the sea state changes from low to high, the ship's mean velocity increases. Since the vehicle starts with the same initial velocity in all cases, the relative speed between the vehicle and the ship decreases as the sea state is changed from low to high. With a fixed landing time of 40 seconds and decreasing relative speed, a higher number of resulting trajectories fall within acceptable error limits as the sea state changes from low to high.

Effect of External Disturbances

The trajectory solution results obtained with the point mass model showed the performance of MPPI without any external disturbances, such as ship air wake, etc. In order to evaluate the MPPI solution in the presence of external random disturbances, which is a representation of the turbulence due to ship airwake, Gaussian noise with zero mean and standard deviation σ (value changes with sea state) is introduced as a disturbance for both X- and Z- axes in Eq. 3 to represent the truth model. Thus, the onboard model is represented by Eq. 3 while the truth model becomes

$$\begin{bmatrix} \dot{z} \\ \dot{w} \\ \dot{a} \end{bmatrix} = \begin{bmatrix} 0 & 1 & 0 \\ 0 & 0 & 1 \\ 0 & 0 & -\frac{1}{\tau} \end{bmatrix} \begin{bmatrix} z \\ w \\ a \end{bmatrix} + \begin{bmatrix} 0 \\ 0 \\ \frac{a_c}{\tau} \end{bmatrix} + \begin{bmatrix} 0 \\ 0 \\ \frac{v}{\tau} \end{bmatrix} \tag{9}$$

where $v \sim \mathcal{N}(\mu = 0, \sigma^2 = 0.25)$ for low sea state, $v \sim \mathcal{N}(\mu = 0, \sigma^2 = 1)$ for medium sea state and $v \sim \mathcal{N}(\mu = 0, \sigma^2 = 1.56)$ for high sea state. In this case, the actual vehicle state from the truth model at the current time instant is taken as the initial state for the updated MPPI solution with the predictive model.

The representative results for a moving ship with random ship deck motion for medium sea state with disturbance introduced in the truth model are shown in Figs. 10 through 12. As shown in Fig. 1, the vehicle starts the landing from a height of 100 ft above and 1100 ft behind the ship deck with an X velocity of 95.4 ft/s.

Figures 10 through 12 show that although there are deviations due to the disturbance compared to the case without

Table 2. X and Z axis position and velocity errors, and usable number of trajectories averaged over 30 simulations [point mass model].

		Sea State		
		Low	**Medium**	**High**
X-Axis	Final Position Error (ft)	1.14	0.76	0.63
	Final Velocity Error (ft/s)	0.25	0.18	0.40
	Avg. No. of Usable Trajs.	65.2	83.8	93.8
Z-Axis	Final Position Error (ft)	0.31	0.55	1.56
	Final Velocity Error (ft/s)	0.28	0.28	0.42
	Avg. No. of Usable Trajs.	99.8	99.8	99.7

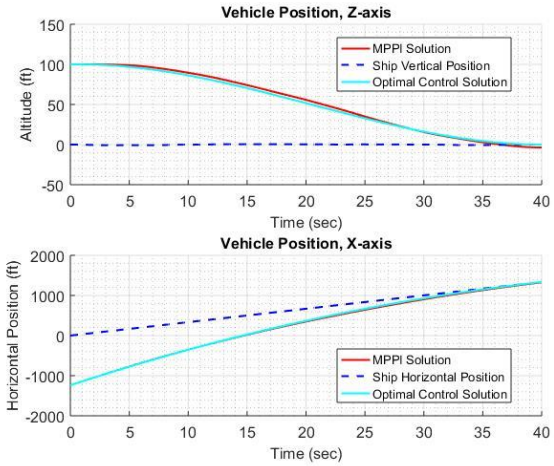

Figure 10. Vehicle positions (MPPI and optimal control solutions) and ship deck positions in the X, Z-axes for random ship deck motion with disturbance in the truth model [point mass model].

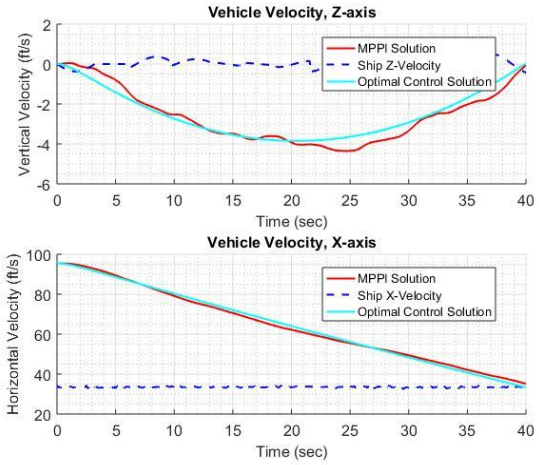

Figure 11. Vehicle velocities (MPPI and optimal control solutions) and ship deck velocities in the X, Z-axes for random ship deck motion with disturbance in the truth model [point mass model].

disturbance (Figs. 5 through 9), the MPPI method performs satisfactorily despite differences between the truth and online models.

Table 3 shows the results for all the sea states, each averaged over 30 simulations with disturbance introduced in the truth model. It is seen that the position and velocity errors are higher compared to the disturbance-free case (Table 2). This is expected since the prediction or onboard model does not account for disturbance explicitly and the calculated control input will not yield a similar response when given to the truth model. The position errors are significantly higher since the disturbance introduced in acceleration gets integrated twice compared to velocity. It is also observed that the position errors decrease with sea state in X axis, for the same reasons as explained earlier, while the position errors increase with sea state in the Z axis due to higher variance in the disturbance signal.

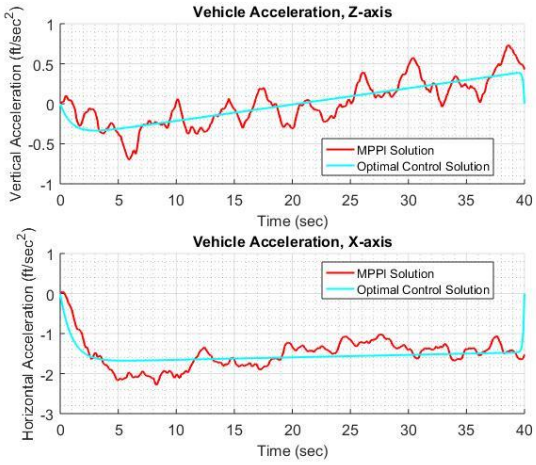

Figure 12. Vehicle accelerations (MPPI and optimal control solutions) in the X, Z-axes for random ship deck motion with disturbance in the truth model [point mass model].

MPPI USING A LINEAR HELICOPTER MODEL

The simple first order model serves as a good reference to perform initial studies. The proof-of-concept using MPPI approach for trajectory guidance in shipboard landing is explored next using a helicopter model. This section elaborates the details of using a linearized helicopter model in forward flight (trimmed at a particular airspeed) considering random ship deck motion. Two cases of ship landing are considered – A) without any lateral offset, i.e. the helicopter is lined up with the course of the ship, and B) with lateral offset, where the helicopter approaches the ship from the port side. The landing is completed with a fixed time of 40 seconds for both cases. A sketch of Case A landing is shown earlier in Fig. 1. A sketch of Case B landing in medium sea state is shown in Fig. 13.

The truth model as well as onboard model for prediction are the same linearized model of the UH-60 helicopter obtained from FLIGHTLAB®, a high-fidelity industry-standard tool for rotorcraft flight dynamics modelling and analysis (Ref. 11). The vehicle is trimmed in forward flight at 40 knots (67.5 ft/s) airspeed and the corresponding linear model obtained is of the form

$$\dot{x} = Ax + Bu \tag{10}$$

where x is the vector of helicopter states (body axes) and u is the control inputs vector.

An initial estimate for the control profile is obtained again from optimal control theory. However, the performance measure in this case cannot be chosen as minimizing control effort alone as it could result in impractical trajectories. Thus, a quadratic penalty function is chosen to include cost terms penalizing deviations in following a desired trajectory (see Eq. 11).

Table 3. X and Z axis position and velocity errors, and usable number of trajectories averaged over 30 simulations with disturbance introduced [point mass model].

		Sea State		
		Low	**Medium**	**High**
X-Axis	Final Position Error (ft)	14.58	13.52	12.11
	Final Velocity Error (ft/s)	1.08	1.34	1.93
	Avg. No. of Usable Trajs.	37.0	53.1	53.6
Z-Axis	Final Position Error (ft)	2.98	7.93	22.41
	Final Velocity Error (ft/s)	0.70	1.00	1.92
	Avg. No. of Usable Trajs.	92.8	68.3	52.6

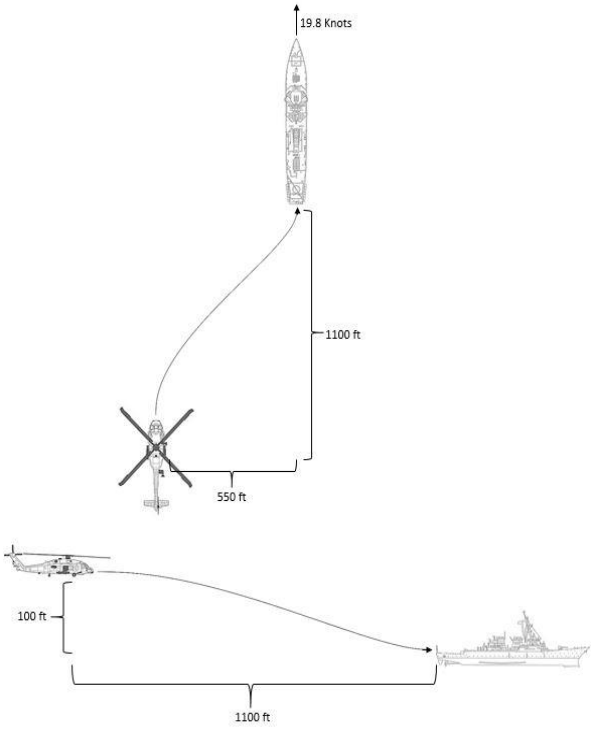

Figure 13. Landing phase with lateral offset.

$$J = \frac{1}{2}\int_{t_0}^{t_f}[(z - Cx)^T Q(z - Cx) + u^T Ru]dt \qquad (11)$$

where x and u represent the states and control inputs of the model. z represents the reference trajectory (position and velocity) to be followed in the inertial coordinates and C represents the matrix for obtaining the corresponding inertial quantities from the state vector x. Q is the weighting matrix for error between the desired and actual vehicle response and R is the weighting matrix for control effort. For this trajectory following problem, the control law is based on linear state feedback to follow a desired output as elaborated in Ref. 12.

The reference trajectories can be generated using multiple techniques. A simple approach which has been adopted is using the trajectories generated with the point mass vehicle represented in the form of a first order acceleration model (Eq. 3) from solving the boundary value problem for a fixed terminal ship deck by minimizing vehicle accelerations as described in the previous section. Thus, reference trajectories (generated independently for all the axes) for inertial positions and velocities are obtained and used to calculate the optimal control profile which serves as the initial value for the control vector required in the MPPI approach.

With an initial estimate for the control vector in MPPI thus obtained, the same performance measure as shown in Eq. 11 augmented with terminal cost terms (see Eq. 12) is selected for evaluating the helicopter controls during landing, using the optimal trajectories obtained using the point mass model as reference. The number of random control vectors or trajectories is maintained at M = 100 with a time step of Δt = 0.1 s. A brief study was conducted by increasing M from 100 to 500 in steps of 100 to determine the effect of number of random control vectors on the performance measure and terminal errors. However, the values were not very different, which led to M being fixed at 100. The random control perturbations are kept at 10% for all control inputs. Similar to the number of control vectors, a simple analysis on the effect of random control perturbation magnitude was carried out by changing the values from 5% to 20%. This analysis also did not show any significant change in the performance cost or terminal errors, so 10% was chosen. It is important to note that since the model is coupled in the X, Y and Z axes, the entire MPPI evaluation is done together for all degrees of freedom as opposed to the simple model where individual axis was evaluated separately. Trajectories which yielded terminal position and velocity errors more than 5 ft and 3 ft/s in all three axes simultaneously were rejected. Note that this specific rejection criterion used, where trajectories with terminal errors outside the selected bounds in one or two axes would be allowed, could result in a degraded MPPI solution. This aspect on how to devise a more robust rejection criterion needs to be addressed in the future. It was also observed that only a single iteration occurred at each time step for the entire duration when the linear helicopter model is tested.

Results for Zero Lateral Offset Approach (Case A Landing)

This section presents the results for ship landing with no lateral offset (see Fig. 1 for a sketch) using the linear model. Hence, the truth as well as onboard models have the state and control vectors

$$x = [X \quad Y \quad Z \quad \varphi \quad \theta \quad \psi \quad u_b \quad v_b \quad w_b \quad p \quad q \quad r]^T$$

and $u = [\delta_b \quad \delta_a \quad \delta_p \quad \delta_c]^T$ respectively, with the reference trajectory vector as

$$z = [U_{ref} \quad V_{ref} \quad W_{ref} \quad X_{ref} \quad Y_{ref} \quad Z_{ref}]^T$$

The methodology is the same as elaborated before except the performance measure, which now becomes

$$J_i = \frac{1}{2}\int_{t_j}^{t_f} [(z - Cx)^T Q(z - Cx) + u^T R u]dt + F\left(\left(Z_h(t_f) - Z_s(t_f)\right)^2 + \left(W_h(t_f) - W_s(t_f)\right)^2\right) \quad (12)$$

The weighting function F is logarithmically spaced 10^{-2} to $10^{0.5}$ as indicated previously to give more importance to the terminal conditions as the helicopter gets closer to the ship deck. Note that the range of F used with the helicopter model is different from that used with the point mass model due to the additional term in path cost associated with following a reference trajectory. In Eq. 12, the first term represents the path cost which is the same for all degrees of freedom while the second term represents the terminal cost which is different for X, Y and Z axes. The reference trajectories for X and Z inertial axes are generated using the same point-mass model represented as a first order command acceleration model independently, while the reference trajectories for Y axis are maintained at zero. It is important to note that pedal control is included in the control cost term in the performance index but there is no contribution of heading in the trajectory-following cost or terminal cost.

Figures 14 through 17 portray the results for the linear helicopter model for zero lateral offset ship landing approach in medium sea state with shrinking horizon optimization method. The vehicle starts the landing phase from a height of 100 ft above and 1100 ft behind the ship deck with a velocity of 67.5 ft/s. It is observed that the MPPI results closely match the reference trajectories and the position and velocity in Y axis do not change much throughout the landing with a peak value of 5 ft and 2 ft/s respectively towards the end.

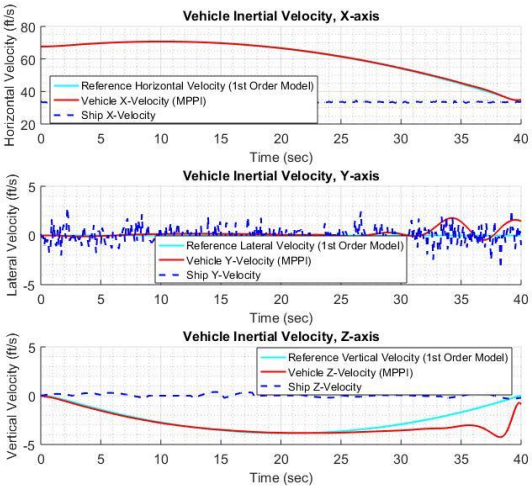

Figure 15. Vehicle velocities (MPPI) and ship deck velocities with reference trajectories in the X, Y, Z-axes for zero lateral offset (shrinking horizon) [6-DOF helicopter linear model].

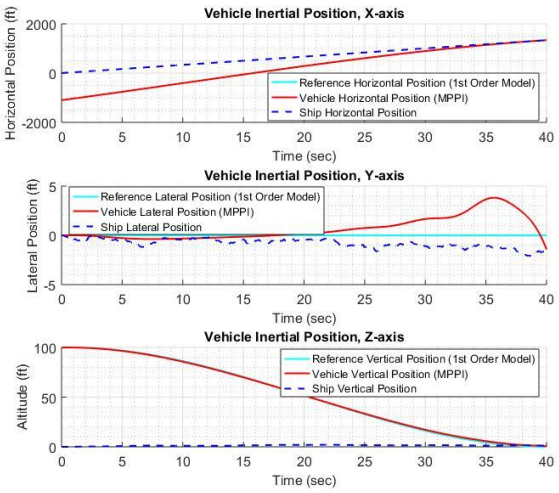

Figure 14. Vehicle positions (MPPI) and ship deck positions with reference trajectories in the X, Y, Z-axes for zero lateral offset (shrinking horizon) [6-DOF helicopter linear model].

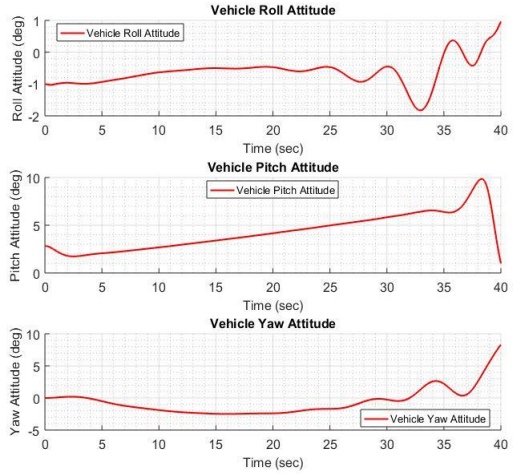

Figure 16. Vehicle attitude (MPPI) for zero lateral offset (shrinking horizon) [6-DOF helicopter linear model].

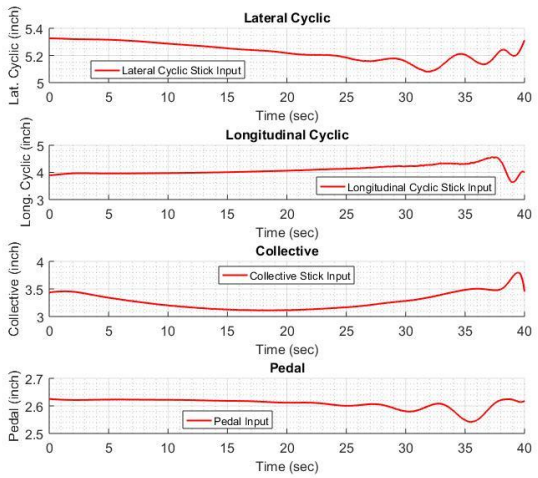

Figure 17. Vehicle controls (MPPI) during landing for zero lateral offset (shrinking horizon) [6-DOF helicopter linear model].

On observing Fig. 16, it is noted that there is a sharp pitch attitude change towards the end of the landing. This is because the reference trajectory is generated for a point mass vehicle represented as a first-order command acceleration model, which does not have any attitude considerations while minimizing accelerations. Hence, the generated trajectories in positions have a near constant slope except towards the end where there is a distinct curve, which causes a sharp pitch up in order to maintain the reference position and velocity profiles. As a result, the vertical velocity is also affected due to its dependence on pitch attitude (Fig. 15). No constraints are placed on attitude but the maximum pitch attitude stays within an acceptable limit of 15 degrees. Furthermore, the roll attitude changes by a maximum of 2 degrees from the trim value at the terminal time. Similarly, the heading angle does not vary significantly except close to the terminal time as no heading constraints are included. The control input changes are significant in longitudinal cyclic and collective, compared to the lateral cyclic and pedal (see Fig. 17).

Table 4. X, Y and Z axes terminal position and velocity errors averaged over 20 simulations for complete linear helicopter model with moving ship deck and zero lateral offset (shrinking horizon) [6-DOF helicopter linear model].

		Sea State		
		Low	**Medium**	**High**
X-Axis	Final Position Error (ft)	0.41	0.50	1.48
	Final Velocity Error (ft/s)	3.70	1.06	0.46
Y-Axis	Final Position Error (ft)	1.14	1.02	2.43
	Final Velocity Error (ft/s)	10.10	1.49	0.66
Z-Axis	Final Position Error (ft)	0.68	0.74	1.60
	Final Velocity Error (ft/s)	1.17	0.78	0.70

Table 4 summarizes the results for zero lateral offset ship landing for the linear model with shrinking horizon optimization averaged over 20 simulations in each sea state. The average number of usable trajectories remains at 99.75 (out of 100) with an average running time per simulation of 31.05 s. The position and velocity terminal errors are well within the limits of 5 ft and 3 ft/s respectively for both medium and high sea states. It is observed that the Y-axis position and velocity errors are higher compared to the X and Z axes, particularly for the low sea state case, perhaps because the reference trajectory does not account for any heading changes and roll-yaw coupling. The low sea state is the furthest away in terms of relative speed of the helicopter with respect to the ship, leading to a steeper change in the reference trajectory, which subsequently affects the helicopter response as it tries to maintain the given trajectory, thereby leading to larger errors. Also, the specific rejection criterion used in this study, where those trajectories with terminal errors outside the selected bounds simultaneously in all three axes alone were rejected, could lead to degraded MPPI solutions. This is noticed in Table 4 results in the X- and Y- axes terminal velocity errors for the low sea state case.

Shrinking vs Receding Horizon for Optimization

The MPPI approach incorporated until now predicts and optimizes from the current instance t_j until the end of the landing task t_f in discrete time steps Δt, which is detailed earlier. This is referred to as the shrinking horizon since the horizon or window of prediction and optimization continues shrinking until the last time step. This approach is satisfactory as long as the prediction or onboard model is accurate and is similar to the truth model. However, this is not necessarily the case in actual application since the truth model is the actual helicopter, which can be different from the onboard model. Hence, predicting and optimizing till the terminal time using the onboard model will involve loss of fidelity for long horizon predictions while increasing the computational cost.

A suitable alternative is to consider a receding horizon. In this approach, a short time window is selected, say t_{win} = 2 s, and the prediction and optimization are done only for this duration. Thus, starting at t_0, the vehicle response using the onboard model is predicted only from t_0 to $t_0 + t_{win}$ in steps of Δt, instead of t_0 to t_f as in the shrinking horizon case. Once the control is evaluated and given as input to the truth model for Δt, the process is repeated again with the short window moving as $t_0 + \Delta t$ to $t_0 + \Delta t + t_{win}$, with increments by Δt until $t_0 + n\Delta t + t_{win} = t_f$. After this, the short window can no longer

move ahead since it is bounded by the terminal time, hence the shrinking horizon optimization takes over from $t_0 + n\Delta t$ until t_f. Therefore, the terminal constraints do not contribute to the performance measure until the short horizon reaches the end where the ship deck is close by. The performance measure for the current approach is rewritten as

$$J_i = \frac{1}{2}\int_{t_j}^{t_j + t_{win}} [(z - Cx)^T Q(z - Cx) + u^T Ru]dt, \quad when\ t_j + t_{win} < t_f \tag{13a}$$

$$J_i = \frac{1}{2}\int_{t_j}^{t_f} [(z - Cx)^T Q(z - Cx) + u^T Ru]dt + F\left(\left(Z_h(t_f) - Z_s(t_f)\right)^2 + \left(W_h(t_f) - W_s(t_f)\right)^2\right), \quad when\ t_j + t_{win} = t_f \tag{13b}$$

Figures 18 through 21 depict the landing phase with a short receding horizon for optimization with zero lateral offset approach in medium sea state. On comparing these results with those shown for the shrinking horizon (Figs. 14 through 17), it is evident that there are no significant changes. However, it can be subtly noted that the positions and velocities match the reference trajectories better for the shrinking horizon case, which is expected since the performance measure does not include any terminal costs until the end for the receding horizon. This also leads to a slightly lower path cost for the receding horizon compared to the shrinking horizon. This could further explain the smoother control profiles in the receding horizon case compared to the shrinking horizon approach. Since receding horizon technique results in higher terminal errors compared to shrinking horizon due to the introduction of terminal cost only towards the end, the control perturbations are reduced from 10% to 1% for the lateral cyclic and pedal inputs in the receding horizon method to attain satisfactory terminal errors.

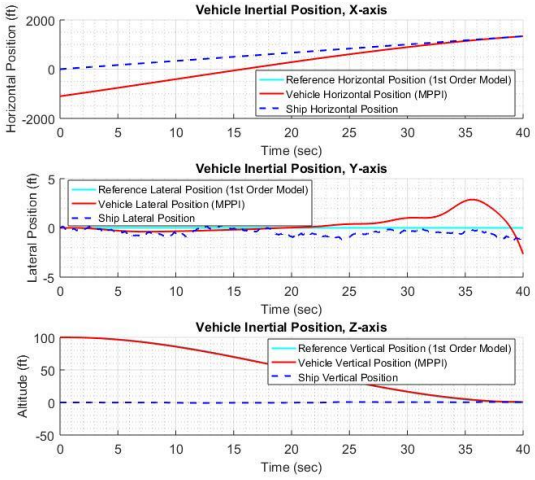

Figure 18. Vehicle positions (MPPI) and ship deck positions with reference trajectories in the X, Y, Z-axes for zero lateral offset (receding horizon) [6-DOF helicopter linear model].

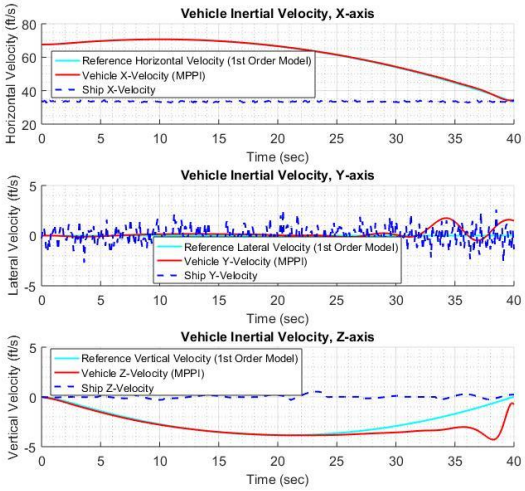

Figure 19. Vehicle velocities (MPPI) and ship deck velocities with reference trajectories in the X, Y, Z-axes for zero lateral offset (receding horizon) [6-DOF helicopter linear model].

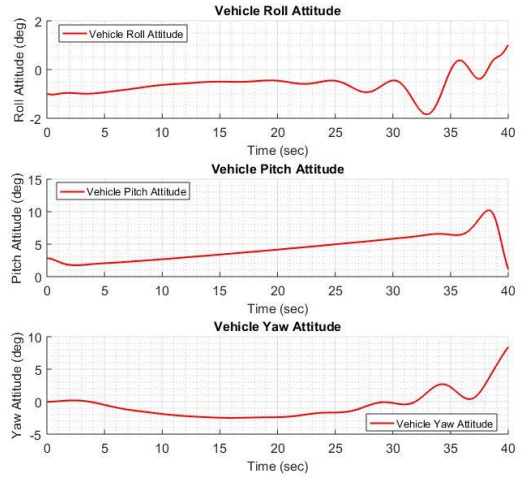

Figure 20. Vehicle attitude (MPPI) for zero lateral offset (receding horizon) [6-DOF helicopter linear model].

Table 5 summarizes the receding horizon results for all sea states, each averaged over 20 simulations. The starting conditions and other parameters are the same for both shrinking and receding horizon approaches. It is observed that the terminal errors are slightly higher compared to the shrinking horizon approach which is expected since the terminal constraint contributions appear only towards the end. However, the position and velocity errors are still within the acceptable limits of 5 ft and 3 ft/s respectively in medium and high sea states. As explained before for the MPPI solution with the shrinking horizon, the relatively large terminal lateral axis position and velocity errors for the low sea state case seen in Table 5 could be attributed to the specific rejection criterion used in obtaining the MPPI solution. A significant difference is noted with the average running time per simulation, which is around 6.66 seconds for the receding horizon. This

substantial reduction in time from the shrinking horizon method makes the receding horizon approach better for saving on computational time.

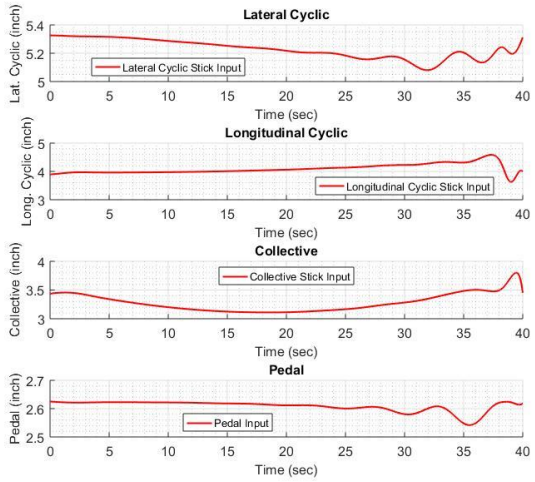

Figure 21. Vehicle controls (MPPI) during landing for zero lateral offset (receding horizon) [6-DOF helicopter linear model].

Table 5. X, Y and Z axes terminal position and velocity errors averaged over 20 simulations for linear helicopter model with moving ship deck and zero lateral offset (receding horizon) [6-DOF helicopter linear model].

		Sea State		
		Low	**Medium**	**High**
X-Axis	Final Position Error (ft)	1.70	2.23	3.36
	Final Velocity Error (ft/s)	3.51	0.92	0.81
Y-Axis	Final Position Error (ft)	6.32	2.62	3.71
	Final Velocity Error (ft/s)	10.12	1.55	2.11
Z-Axis	Final Position Error (ft)	0.62	1.21	2.30
	Final Velocity Error (ft/s)	1.38	0.80	0.76

Results for Lateral Offset Approach (Case B Landing)

This section presents sample results with the linear model of the helicopter for a ship landing with a lateral offset.

The reference trajectories for X, Y and Z axes are generated independently using the first order acceleration model as described by Eq. 3. The number of random control vectors is 100 and the random control perturbations are 10% for all the four controls. The helicopter starts at 1100 ft behind, 100 ft above and 550 ft to the left of the ship in the inertial frame and completes the landing in 40 seconds (see Fig. 13).

Figures 22 through 25 present the results for shrinking horizon approach in medium sea state with random deck motion, while Figs. 26 through 29 depict the corresponding results for the receding horizon approach. The representative results for the receding horizon are similar to the shrinking horizon as mentioned previously, with higher terminal position and velocity errors.

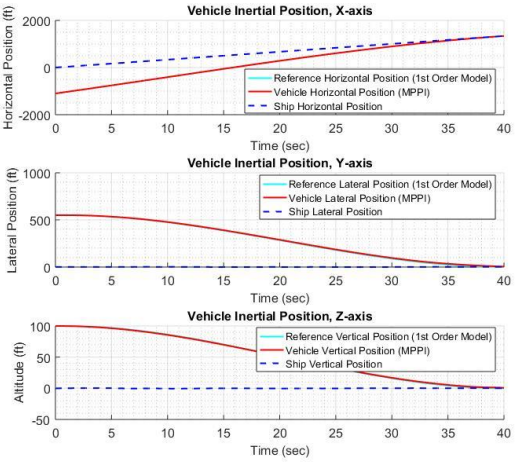

Figure 22. Vehicle positions (MPPI) and ship deck positions with reference trajectories in the X, Y, Z-axes with lateral offset landing (shrinking horizon) [6-DOF helicopter linear model].

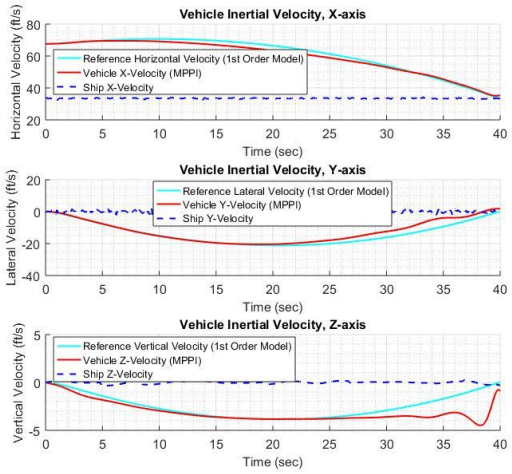

Figure 23. Vehicle velocities (MPPI) and ship deck velocities with reference trajectories in the X, Y, Z-axes with lateral offset landing (shrinking horizon) [6-DOF helicopter linear model].

As seen in Figs. 22 and 23, the vehicle positions and velocities follow the reference trajectories closely in all axes, with slight offsets towards the end due to significant roll and pitch angles close to landing. Since the heading of the helicopter is initially

at 0 deg (same heading as ship deck), the heading continues to change with the reference trajectory curvature and lands with a heading of 10 deg relative to the ship deck (as shown in Fig. 24) due to the lack of any terminal heading constraints. Oscillations in roll and yaw angles (see Fig. 24) are prominent as the curvature of the Y-axis trajectory changes to maintain the given Y-velocity profile, which is also visible in the corresponding control inputs (Fig. 25). Similar trends are observed for the receding horizon results (Figs. 26 through 29).

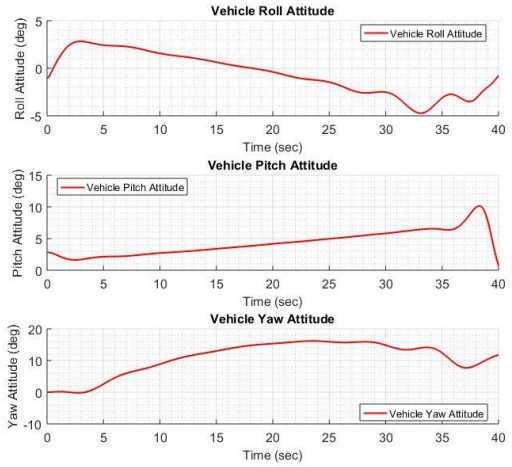

Figure 24. Vehicle attitude (MPPI) with lateral offset landing (shrinking horizon) [6-DOF helicopter linear model].

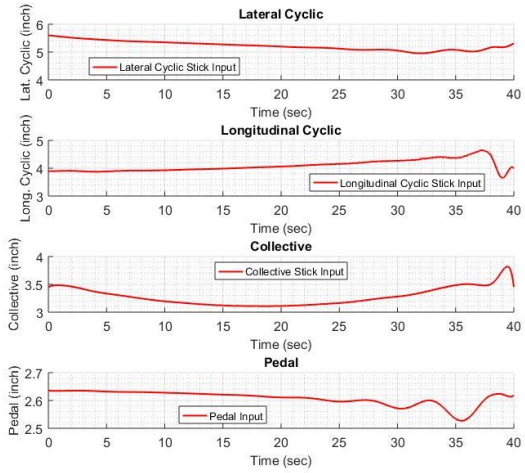

Figure 25. Vehicle controls (MPPI) during lateral offset landing (shrinking horizon) [6-DOF helicopter linear model].

Tables 6 and 7 present the results for all sea states, each averaged over 20 simulations, for the shrinking horizon and receding horizon approaches, respectively. It is observed that the errors are higher for the receding horizon case compared to the shrinking horizon case due to terminal constraints contribution only towards the end. An additional observation is the higher errors in Y-axis position and velocity compared to the X and Z axes, particularly for the low sea state case.

Table 6. X, Y and Z axes terminal position and velocity errors averaged over 20 simulations for linear helicopter model with moving ship deck for lateral offset approach (shrinking horizon) [6-DOF helicopter linear model].

		Sea State		
		Low	**Medium**	**High**
X-Axis	Final Position Error (ft)	0.91	0.52	1.4
	Final Velocity Error (ft/s)	5.07	1.72	0.75
Y-Axis	Final Position Error (ft)	1.26	1.04	2.75
	Final Velocity Error (ft/s)	11.76	1.73	1.44
Z-Axis	Final Position Error (ft)	0.57	0.71	1.48
	Final Velocity Error (ft/s)	1.13	0.84	0.81

Table 7. X, Y and Z axes terminal position and velocity errors averaged over 20 simulations for linear helicopter model with moving ship deck for lateral offset approach (receding horizon) [6-DOF helicopter linear model].

		Sea State		
		Low	**Medium**	**High**
X-Axis	Final Position Error (ft)	2.63	1.92	3.33
	Final Velocity Error (ft/s)	5.06	1.23	0.89
Y-Axis	Final Position Error (ft)	18.12	7.14	5.05
	Final Velocity Error (ft/s)	12.12	1.69	2.10
Z-Axis	Final Position Error (ft)	0.99	1.12	1.62
	Final Velocity Error (ft/s)	1.30	0.89	1.08

This is because the reference trajectory generated does not consider roll-yaw coupling in the vehicle approach. Furthermore, the specific rejection criterion used in this study, where only those trajectories with terminal errors outside the selected bounds simultaneously in all three axes are rejected, could lead to a degraded MPPI solution. This is noticed in

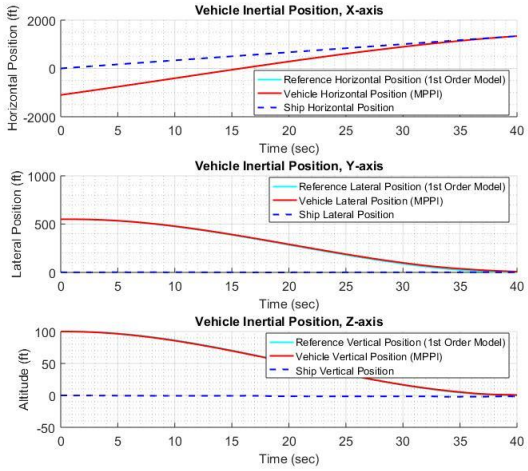

Figure 26. Vehicle positions (MPPI) and ship deck positions with reference trajectories in the X, Y, Z-axes with lateral offset landing (receding horizon) [6-DOF helicopter linear model].

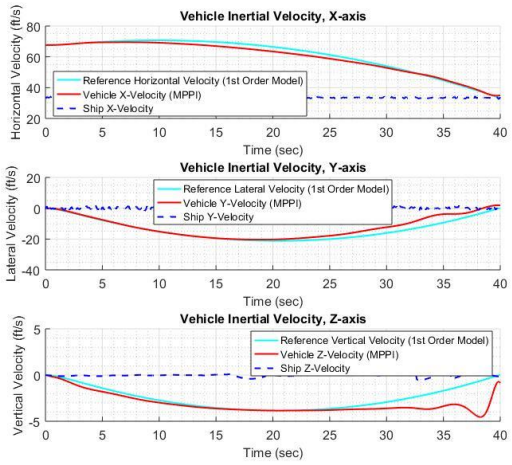

Figure 27. Vehicle velocities (MPPI) and ship deck velocities with reference trajectories in the X, Y, Z-axes with lateral offset landing (receding horizon) [6-DOF helicopter linear model].

results of Tables 6 and 7, especially in the Y-axis terminal errors and X-axis terminal velocity error for the low sea state case.

Table 8 from Ref. 13 provides a few landing quality metrics for shipboard landing controller design. According to this table, the current MPPI algorithm with a coupled linear helicopter model achieves Level 1 for medium and high sea states in the shrinking horizon method for both zero and non-zero lateral offset landing. For the case of receding horizon, due to the large errors in Y-axis, Level 3 is achieved in medium sea state and Level 2 in high sea state for the non-zero lateral offset landing. The receding horizon method achieves Level 1 in medium sea state and Level 2 in high sea state for the landing with zero lateral offset. While these results are illustrative of the MPPI perfromance, the large errors seen in Y-axis can be redcued by using reference

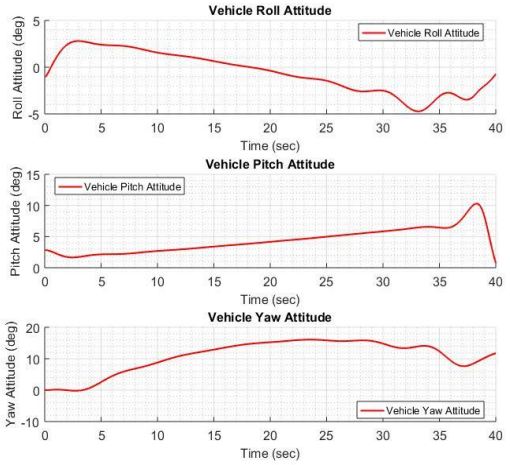

Figure 28. Vehicle attitude (MPPI) with lateral offset landing (receding horizon) [6-DOF helicopter linear model].

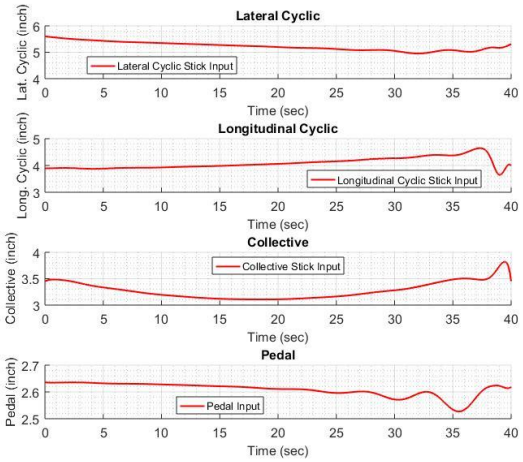

Figure 29. Vehicle controls (MPPI) during lateral offset landing (receding horizon) [6-DOF helicopter linear model].

trajectories that take into account lateral-yaw coupling and through appropriate fine-tuning of the weighting placed on the terminal cost terms in the MPPI solutions.

CONCLUDING REMARKS

The paper explores the application of using Model Predictive Path Integral (MPPI) approach, a stochastic optimal control technique, for trajectory guidance in rotorcraft shipboard landing. First, a proof-of-concept study is carried out by using a simple point mass approximation of vehicle dynamics represented as a first order command acceleration model with two independent degrees of freedom. While an explicit representation of air wake model is not considered, an initial exploration of the MPPI performance in the presence of random variations in vehicle accelerations due to external gust disturbances is performed. The performance of the MPPI method is further explored using a six degrees-of-freedom linearized helicopter model and for two cases of landing

Table 8. Landing Quality Metrics for Shipboard Control Design (Ref. 13).

	Level 1	Level 2	Level 3
Touchdown Longitudinal Position Error (ft)	± 4	± 6	± 8
Touchdown Lateral Position Error (ft)	± 4	± 6	± 8
Touchdown Lateral Velocity Error (ft/s)	≤ 2	≤ 4	≤ 6
Touchdown Vertical Velocity Error (ft/s)	≤ 2	≤ 4	≤ 6

profiles. Two cases of optimization time windows are investigated – a shrinking window in which the optimization is performed from the current time to the terminal time and a receding horizon in which the optimization is performed over a selected width of moving window.

From the results obtained in this study, it is seen that the MPPI method, despite being an implicit method of optimization, provides optimal control solutions comparable to optimal control theory based explicit methods, while significantly reducing computational time, thus making it a viable candidate for real time guidance and control. From a comparison of results obtained for the shrinking horizon and receding horizon approaches, it is seen that the receding horizon approach further reduces the computational time with only a slight degradation in meeting the terminal constraints. The specific rejection criterion in stochastic averaging of sample trajectories, where the sample trajectories with terminal errors outside the selected bounds in all axes simultaneously alone were rejected, led to degraded MPPI solutions, especially in the lateral axis terminal errors for the low sea state case.

The proof-of-concept study considered only trajectory errors in the performance index and no explicit representation of air wake effects. Future study will consider inclusion of other metrics, such as vehicle attitudes constraints, rotor torque limit, etc., and with representative air wake models and random ship deck motions that include, in addition to the heaving motion considered in the present study, pitching and rolling motions. Also, the aspect of devising a more robust criterion for the rejection of sample trajectories with terminal errors outside selected bounds will be investigated in the future. Further, future work will include piloted simulation evaluations of ship board landings with MPPI trajectory guidance.

Author contact:
J. V. R. Prasad jvr.prasad@ae.gatech.edu
Vinodhini Comandur vinodhini@gatech.edu
Robert Walters rwalters31@gatech.edu
David Guerrero dguerrero555@gmail.com

ACKNOWLEDGMENTS

This study is supported under the NRTC Vertical Lift Rotorcraft Center of Excellence (VLRCOE) from the U.S. Army Aviation and Missile Research, Development and Engineering Center (AMRDEC) under Technology Investment Agreement W911W6-17-2-0002, entitled Georgia Tech Vertical Lift Research Center of Excellence (GT-VLRCOE) with Dr. Mahendra Bhagwat as the Program Manager. The authors would like to acknowledge that this research and development was accomplished with the support and guidance of the NRTC. The views and conclusions contained in this document are those of the authors and should not be interpreted as representing the official policies, either expressed or implied, of the AMRDEC or the U.S. Government. The U.S. Government is authorized to reproduce and distribute reprints for Government purposes notwithstanding any copyright notation thereon.

REFERENCES

[1]Bradley, R. and Turner, G. "Simulation of the human pilot applied at the helicopter/ship dynamic interface," American Helicopter Society 55th Annual Forum, Montreal, Canada, May 1999.

[2]Turner, G., Brindley, G. and Bradley, R. "Simulation of pilot control activity for the prediction of workload ratings in helicopter/ship operations," 26th European Rotorcraft Forum, The Hague, Netherlands, September 2000.

[3]Hess, R.A., "A Simplified Technique for Modeling Piloted Rotorcraft Operations Near Ships," AIAA Atmospheric Flight Mechanics Conference and Exhibit, San Francisco, California, Aug. 15-18, 2005. AIAA-2005-6030.

[4]Lee, D. and Horn, J.F., "Simulation of Pilot Workload for a Helicopter Operating in a Turbulent Ship Airwake." *Journal of Aerospace Engineering – Proceedings of the Institute of Mechanical Engineers Part G*, Special issue on shipborne aviation, Vol. 219, November 2005, pp. 445-458.

[5]Wu, A. D., Johnson, E. N., and Proctor, A. A., "Vision Aided Inertial Navigation for Flight Control," AIAA Guidance, Navigation and Control Conference, San Francisco, California, August 2005.

[6]Langelaan, J. W., "State Estimation for Autonomous Flight in Cluttered Environments," *Journal of Guidance, Control and Dynamics*, Vol. 30, (5), September-October 2007, pp. 1414–1426.

[7]Horn, J. F., He, C., Tritschler, J. K., et. al. "Autonomous Ship Approach and Landing using Dynamic Inversion Control with Deck Motion Prediction," 41st Annual European Rotorcraft Forum Proceedings, Munich, Germany, September 2015.

[8]Shin, H., You, D., and Shim, D. H., "Autonomous Shipboard Landing Algorithm for Unmanned Helicopters in Crosswind", *Journal of Intelligent & Robotic Systems*, Vol. 74, Issue 1-2, April 2014, pp 347-361. doi: 10.1007/s10846-013-9927-2

[9]Tritschler, J. K., Horn, J. F., and He, C., "Objective Function Development for Optimized Path Guidance for Rotorcraft Shipboard Recovery," Paper AIAA 2015-2395, AIAA Atmospheric Flight Mechanics Conference Proceedings, AIAA Aviation Forum, Dallas, TX, June 2015.

[10]Williams, G., Aldrich, A. and Theodorou, E. A., "Model Predictive Path Integral Control: From Theory to Parallel Computation," *Journal of Guidance, Control, and Dynamics*, Vol. 40, No. 2, Feb. 2017, pp. 344-357. doi: 10.2514/1G001921

[11]FLIGHTLAB XAnalysis User Manual, Advanced Rotorcraft Technology, Inc., July 2013.

[12]Bryson Jr., A. E., and Ho, Y.-C., "Linear feedback to follow a desired output," *Applied Optimal Control: Optimization, Estimation and Control*, Chap. 5, CRC Press, New York, NY, 1975, pp. 175.

[13]Horn, J., He, C., Tritschler, J., et. al. "Autonomous Control Modes and Optimized Path Guidance for Shipboard Landing in High Sea States," Base Effort Final Report (CDRL A002), August 2016.